ORIGINAL ARTICLE

Hook formation and joint strength in friction stir spot welding of Al alloy and Al–Si-coated hot-press forming steel

Minjung Kang[1] · Jinyoung Yoon[1,2] · Cheolhee Kim[1,3]

Abstract

In the automotive industry, the demand for ultra-high-strength steel is increasing due to the CO_2 emission and safety regulations. Hot-press forming (HPF) steels are a type of boron-alloyed high-strength steel fabricated via hot-press forming, which enables both high strength and elongation. Because HPF is conducted at high temperatures (900–950 °C) for a few minutes, its surface is coated with Al–Si or Zn to prevent surface oxidation and decarburizing. However, the coating layer often influences the properties of the welds. In this study, friction stir spot welding (FSSW) is used to weld dissimilar metals, i.e., an Al alloy and Al–Si-coated HPF steel. The effects of Al–Si coating on the mechanical and metallurgical properties of the hook formation on the weld are investigated. The shape of the hook, which is formed during FSSW, changes from bent to straight shape due to the presence of Al–Si and the HPF process. The joint strength of the straight hook-shaped specimens is demonstrated to be lower than that of the bent hook-shaped specimens. This difference in strength is because the hard Fe–Al–Si intermetallic (IMC) layer on the outer surface of the hook disturbs the bending of the hook during the welding. On the outer surface of the hook, a Fe–Al–Si IMC layer of chemical composition similar to that of the coating layer formed during HPF is observed. This formation is different from the inner surface of the hook, wherein a thin Fe–Al IMC layer is reconstructed between aluminum and steel. Thus, the hard Fe–Al–Si intermetallic layer transformed during the HPF process is the primary cause of the straight hook shape.

Keywords Friction stir spot welding · Al/Fe dissimilar metal joint · Hot-press forming steel · Al-Si coating · Intermetallic compound · Hook formation

1 Introduction

Automotive materials are becoming stronger and more diversified. For example, 58% of the structure of the fourth generation spaceframe of Audi A8 is made of aluminum alloys. The rest of the chassis is made of extremely high-strength materials such as hot-press forming (HPF) steel and carbon fiber-reinforced polymer (CFRP) [1]. HPF steels—a type of boron-alloyed high-strength steel—are produced via the hot-press forming process, which enables both high strength and

elongation. HPF steel sheets are into components under temperatures at which ferrite is completely transformed into austenite. During their formation, the sheets in a mold with water cooling channels are quenched; the high temperature improves formability and the simultaneous quenching guarantees a fully martensitic structure [2, 3]. Various welding applications of 1500-MPa grade HPF steel in the automotive industries have been reported using the laser welding [4, 5] and spot welding [6].

When a multi-materials integrated car body is implemented, joining dissimilar materials is of great concern [7–9]. The joining of Al alloy with steel is the most common and important assembly process of dissimilar materials in a multi-materials car body, because Al alloy and steel constitute most of the car body. Although the major welding processes in the automotive industry, conventional fusion welding processes are not preferable for welding dissimilar metals such as Al and Fe because they have different melting points, thermal expansion coefficients, and thermal conductivities. Moreover, the formation of undesirable brittle intermetallic

✉ Cheolhee Kim
  chkim@kitech.re.kr

1   Joining Research Group, Korea Institute of Industrial Technology, Incheon 21999, Korea

2   School of Mechanical Engineering, Hanyang University, Seoul 04763, Korea

3   Department of Mechanical and Materials Engineering, Portland State University, Portland, OR 97201, USA
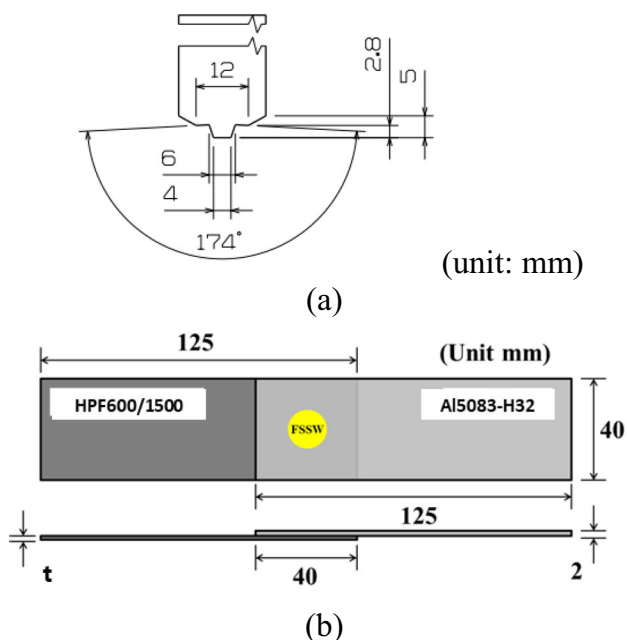
(unit: mm)

(a)

(b)

Fig. 1 Geometry of the applied tool (a) and dimension of welding sample (b) for FSSW

compounds (IMCs) during the welding process, which disrupts the joining [10]. As non-fusion welding processes for the joining of Al/Fe dissimilar metal joint, mechanical joining processes such as self-piercing riveting (SPR) [11, 12], adhesive bonding [7, 13], and friction stir welding (FSW) and friction stir spot welding (FSSW) [14–16] have been largely successful in automotive applications. Among them, FSW and FSSW were recommended as a strong method for joining application of dissimilar materials. FSW and FSSW offer many advantages in the suppression of defects such as blow holes, segregation, cracks, and generation of IMC, compared with conventional welding processes [17].

Hovanski et al. [18] demonstrated FSSW on HPF steel sheet with a tensile strength of 1550 MPa and provided feasibility of the FSSW process for high-strength HPF steel. Santella et al. [19] investigated dissimilar friction stir joining of 780-MPa grade high-strength steel and HPF steel, and Hong et al. [20] evaluated failure mode and fatigue behavior of FSSW specimens. da Silva et al. [21] investigated FSSW of Al 1050 alloy and Al–Si-coated 22MnB5 boron steel using a WC tool. Sound FSSW joint without volumetric defects and reliable tool life were confirmed. However, the 22MnB5 steel

sheet used in the experiments was not heat treated, i.e., the sheet before HPF was used, and its strength was only 582 MPa much lower than 1500 MPa which is expected after HPF of 22MnB5 steel [22].

During friction stir lap welding, a geometric feature called "hook" is formed at the faying surfaces and propagated into the SZ [23]. The hook is generated because of tool penetration into the bottom sheet and upward bending of the sheet interface. The static strength of spot welds is significantly dependent upon the hook geometry, which is influenced by welding parameters such as plunge depth, tool shape [23, 24]. Among the hook geometry, the hook height is known to have the main influence on joint strength of Al/Fe FSSW specimen [25–27]. Since the relationship is complex between the welding parameters and hook shape, it has not been fully understood. Bozzi et al. [24] and Derazkola et al. [28] revealed that the IMCs such as $FeAl_2$, Fe_2Al_5, or $FeAl_3$ are formed around the hook in FSSW of Al and steel, and the formation of IMCs affects the crack propagation path and fracture location. Thus, the hook formation and IMCs distribution have to be evaluated to understand joint strength in FSSW of Al alloy and HPF steel.

In addition, the effects of AlSi coating layer on the properties during the FSSW process is not sufficiently proved. The role of the coating on the surface of the steel plate is reported as the flux and affects the fracture strength and IMC formation behavior [29, 30]. Santella et al. [31] performed FSSW on the uncoated and galvannealed DP780 steel sheets, and reported that Zn coating layer improving the lap shear strength without detrimental effect. However, the AlSi coating thickness increases due to the diffusion of metals during the HPF process. The thickened coating consists of brittle Fe–Al–Si IMCs rather than AlSi, and it is prone to internal Kirkendall voids and cracks [32]. These defects deteriorate cohesion between the coating layer and the base metal, which lowers the adhesive bonding strength [33].

The focus of this study was on the formation of the hooks at the joint interface as well as the morphological changes adjacent to the coating layer before and after welding, and their correlation with the variation of joint strength. This study was conducted to investigate the hook formation after the FSSW process of Al alloy and AlSi-coated HPF steel with 1500 MPa strength. FSSW was performed for Al alloy and both HPF sheets with and without the coating layer which comprises Fe–Al–Si IMCs after HPF.

2 Experimental setup

FSSW was conducted using a three-axis Cartesian FSW welding system (Hwacheon Machinery, F1300, Gwangju, Korea). For details of the welding system and tool height control system, readers are directed to the literature [34, 35]. The tool used for FSSW is made of a WC-Co12% alloy with

Table 1 Chemical compositions of applied hot-press forming steel

Materials	Chemical composition (wt%)						
	C	Si	Mn	P	S	Cr	Fe
HPF600	0.078	0.034	1.64	0.017	0.004	-	Bal.
HPF1500	0.24	0.30	1.21	0.014	0.003	0.20	Bal.

Table 2 Mechanical properties of applied hot-press forming steel

Materials	Before hot-press forming			After hot-press forming			Remarks
	YS (MPa)	TS (MPa)	El (%)	YS (MPa)	TS (MPa)	El (%)	
HPF600	543	589	23	443	694	13	Al–Si coated
HPF1500	427	607	22	1057	1535	7	Al–Si coated

the geometry in Fig. 1a. The pin is conical and unthreaded. If the welding parameters are not specified, the FSSW specimens were made with a rotational speed of 1000 RPM, a feed rate of 20 mm/min, and a dwell time of 9 s. During the experiment, the height control system was used to control the tool to plunge into the lower sheet by a depth of 1 mm.

Al 5083-H32 (thickness = 2.0 mm) and two types of HPF steel—HPF600 (thickness = 1.0 mm) and HPF1500 (thickness = 1.6 mm)—were adopted as the base materials. An aluminum plate was placed on the top and lap-welded upon a HPF steel sheet with an overlap width of 40 mm. As shown in Fig. 1b, the welded specimen was machined for the tensile-shear test according to the ISO 14273 standard.

HPF steels were prepared for both cases before and after heat treatment. During the HPF process, the heating temperature and duration were set to 950 °C and 6 min, respectively, to complete the austenitic phase transformation. The specimens were then quenched inside a water-cooled die in which the water temperature was 20 °C. The chemical composition and mechanical properties of the applied HPF steels are given in Tables 1 and 2, respectively. To evaluate the effect of Al–Si coating, specimens with and without a coating layer were prepared. For the non-coated specimens, the coating layer on the Al–Si-coated sheets was chemically removed using an HCl solution, as shown in Figs. 2a and b, where the coating layer is clearly removed. Before the HPF process, the Al–Si coating layer consisted of a pure Al–Si coating layer, which is shown as the dark gray region including point 1 in Fig. 2c, and a thin Fe–Al–Si interlayer, which is shown as the light gray region including point 2 in Fig. 2c. The total thickness of the coating layer is approximately 20 μm, whereas the average thickness of the Fe–Al–Si IMC layer is 3 μm. During the HPF process, the elements composing the coating layer were diffused into the base metal, causing the average thickness of the layer to increase to over 30 μm (Fig. 2d). Fe from the base metal was also diffused into the coating layer, and its chemical composition gradually decreased according to the distance from the base metal (Table 3).

After the overlap FSSW, the metallurgical and mechanical characteristics were examined. Each specimen was polished and etched with 1% nital solution, and the microstructures of the cross-sectional welds were observed using optical microscopy and field-emission scanning electron microscopy (FE-SEM) systems. Static tensile tests with a strain rate of 0.0012 per second were conducted on the specimen, whose dimensions are shown in Fig. 1b. Three tensile-shear tests were conducted for each condition, and the fracture load was averaged. The micro-Vickers hardness was measured under a load of 0.49 N with a holding time of 20 s.

3 Results and discussion

3.1 Behavior of hook formation according to coating layer

In the FSSW process of Al alloy and Al–Si-coated HPF1500 steel, the HPF process has a noticeable influence on the hook shape (Fig. 3a). A bent hook was observed in the specimen without the HPF process, while a straight upward hook without bending was observed in the HPF-ed specimen. On the other hand, the HPF process did not affect the hook shapes of the welds during the FSSW of Al alloy and non-coated HPF1500 steel (Fig. 3b). The HPF process increased the yield and tensile strengths of the HPF1500 steel by 2.5 times (Table 2) compared with that of the pre-HPF HPF1500 steel. However, the plunge depth did not vary for all cases, and it was not affected by the strengths of the lower steel sheet. An upward hook was confirmed only in one case where the HPF-ed specimen with Al–Si coating was used. As can be seen in Fig. 2 and Table 3, a thick Fe–Al–Si IMC layer is observed only for that case, and the hook shape is (presumably) affected by the IMC layer. To verify the effect of strengths of the base materials, the FSSW of Al alloy and HPF600 steel was conducted, and the same tendency as the HPF1500 steel's as shown in Fig. 4 was confirmed. The hook was bent for other cases, except for the HPF-ed Al–Si-coated specimen. Because the HPF-ed HPF600 steel has a strength less than half of the HPF-ed HPF1500 steel, it is confirmed that the hook shape was affected by the IMC layer rather than material strength.

The evolution of the hook was simulated using various plunge depths from 0.3 to 1.0 mm. Figure 5 shows the macro-sectional images of hook formation with respect to the plunge depth. Bending of the hook was observed even for plunge depths as shallow as 0.3 mm (Fig. 5a). As plunge depth increases, the height of the hook increases, but the change of bending angle at the tip of the hook is not very noticeable. On the contrary, a straight upward hook is observed at all plunge depths during the FSSW of HPF-ed specimens. A schematic diagram of hook formation is illustrated in

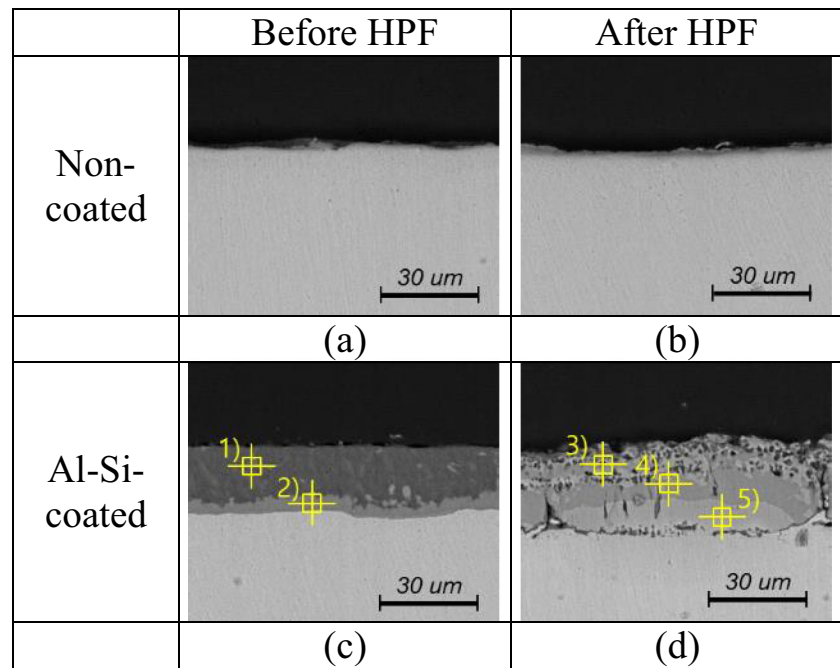**Fig. 2** SEM images of the coating layer on HPF1500 steel before and after hot-press forming

Fig. 6. In the initial state of the tool-plunge phase, the rotating pin caused deformation and material flow, which was localized near the contact area between the pin and the upper plate (Fig. 6(i) to (ii)). When the tool was plunged further into the lower steel sheet, the steel was pushed upwards, and it penetrated the upper Al sheet, which formed a mechanical interlocking, i.e., a hook, between both materials (Fig. 6(iii) to (iv)). After pin retraction, a circular indentation, i.e., pin-hole, remained in the specimen (Fig. 6(v)). The hook formation was strongly related to the driving force generated within the welds. A strong material flow is formed around the pin and shoulder due to the friction force between the tool and the base materials [36]. Yang et al. [36] and Su et al. [37] explained this material flow during FSSW using experimentation and numerical modeling. They stated that the weld metal was stirred upward and outward at the end of the pin. The hook shapes are entirely distinct for both cases even at the initial stage, and the bent hook seemed to be more feasible compared with the

straight one, when considering the flow of metal plasticized at a high temperature. The metallurgical aspects of the hook and its vicinity are discussed in the following section, to reveal the difference in the hook shape.
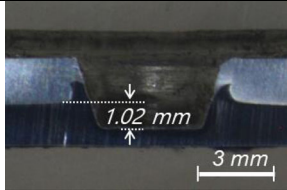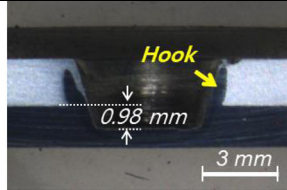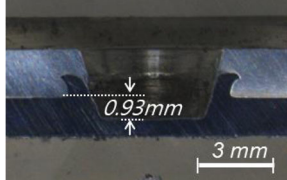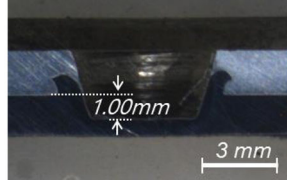
3.2 Intermetallic phase distribution around hook

The Al–Si coating and the HPF process affected the evolution of the hook at the Al alloy–HPF steel interface, and a distinct hook shape, which was straight upward, was found when the Fe–Al–Si IMC layer formed as a result of the HPF process. On the cross-section of the welds, different distributions of the IMC layers were observed for the coated and non-coated specimens. On the one hand, in the case of the non-coated specimen, the IMC layer was observed only along the inner surface of the hook structure, which is indicated by white arrows in Fig. 7. On the other hand, in the case of the coated specimen, the IMC layer was observed not only at the inner surface but also at the outer surface, as indicated by red arrows in Fig. 7b. During the FSSW of steel, the temperature of base materials reached more than 900 °C when a pin was plunged into the steel sheet, which is also demonstrated by Ohishi et al. [38]. This temperature is between the melting temperatures of aluminum and steel, which means that the process temperature of FSSW is sufficient to form the IMCs by diffusion. On the inner surface of the hook close to the rotating tool, it was observed that IMC layers were generated inside the hook with a swirl-layer structure. In the case of the coated specimen, the IMC layer on the inner surface was thicker than that of the non-coated specimen.

Table 3 Measured chemical compositions of coating layer indicated in Figs. 2c and d

Location	Chemical composition (wt%)			
	Al	Si	Mn	Fe
P 1	94.6	5.4	-	-
P 2	56.0	11.8	0.6	31.6
P 3	31.9	8.6	1.4	58.1
P 4	46.1	1.9	2.7	49.3
P 5	25.7	5.5	1.9	66.9

Fig. 3 Macro-sectional images of specimen with and without coating layer and heat treatment for HPF1500 steel
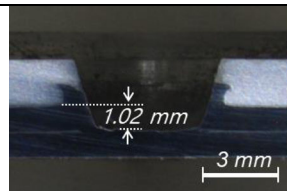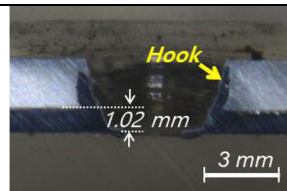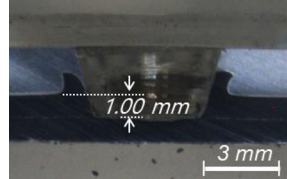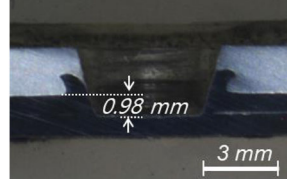

HPF1500 (1.6 mm): rotational speed: 1,000 rpm; dwell time: 9 s; feed rate: 20 mm/min; plunge depth: 1 mm		
Condition	Before HPF	After HPF
(a) Al-Si-coated	1.02 mm / 3 mm	Hook / 0.98 mm / 3 mm
(b) Non-coated	0.93mm / 3 mm	1.00mm / 3 mm

The hardness maps around the hook are presented in Fig. 8. High hardness is observed in the hook made of steel. The hardness value gradually decreases as we move toward the Al matrix. A relatively smooth hardness profile along the boundary of the hook was measured in the non-coated specimen (Fig. 8a), while the hardness was irregularly distributed along the boundary of the hook in the Al–Si-coated specimen. The fluctuation in the hardens map could have originated from the Fe–Al–Si IMCs consisting of the coated layer of the Al–Si-coated specimen. Figure 9 shows the SEM images of the hook and its vicinity in the Al–Si-coated specimen, to reveal the behavior of the Fe–Al–Si IMC layer. The IMC layers were established along both the inner and outer surfaces (Fig. 9b). A relatively thick IMC layer was observed at the tip of the hook compared with other regions (Fig. 9c and d). The IMC layer on the outer surface was crushed into small pieces (Figs. 9c and g), and some part of IMC layers on the outer surface were separated and (probably) mixed within the Al matrix (Fig. 9e and g). The residual IMC layers on the hook's outer surface have a shape similar to that of the coating layer prior to the welding as shown in Fig. 2d. On the boundary, the IMCs that grew toward the steel formed a smooth layer. On the other hand, a swirl-layered structure can be clearly observed on the inner surface of the hook.

The measured chemical composition across the IMC layers is given in Fig. 10. As shown in Table 3, Si element is the element in the coating layer prior to welding. On the outer surface, Si was detected within the IMC layer with a thickness of approximately 35 μm (Fig. 10a), but not in the 6-μm-thick IMC layer on the inner surface (Fig. 10b). Si also was detected in the SZ near the inner surface, which is evidence that the Fe–Al–Si IMC coating layer had scattered from the boundary into the Al matrix during stirring. A considerable amount of Al was detected in the swirl layer inside the hook (Fig. 10b) and the amount of Al element is quite different from that of the Fe–Al–Si IMC layer prior to welding. This observation verified that the swirl

Fig. 4 Macro-sectional images of specimen with and without coating layer and heat treatment for HPF600 steel

HPF600 (1.0 mm): rotational speed: 1,000 rpm; dwell time: 9 s; feed rate: 20 mm/min; plunge depth: 1 mm		
Condition	Before HPF	After HPF
(a) Al-Si-coated	1.02 mm / 3 mm	Hook / 1.02 mm / 3 mm
(b) Non-coating	1.00 mm / 3 mm	0.98 mm / 3 mm

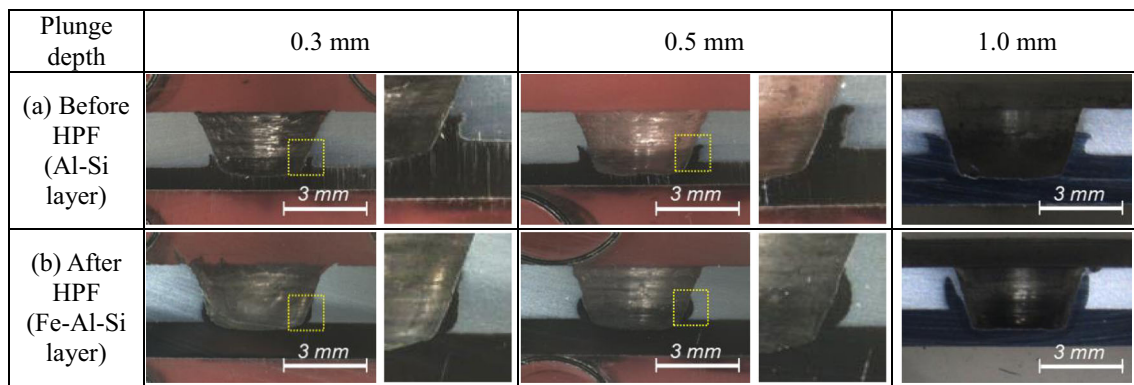| Plunge depth	0.3 mm	0.5 mm	1.0 mm
(a) Before HPF (Al–Si layer)			
(b) After HPF (Fe-Al-Si layer)			

Fig. 5 Behavior of hook formation with respect to plunge depth (welding conditions; Al–Si–coated HPF1500 steel, 1000 RPM rotational speed, 10 mm/min feed rate, 9 s dwell time)

layer and thin IMC layer were reconstructed by diffusion during the FSSW process due to sufficient temperature.

3.3 Relationship between hook shape and fracture load

Figure 11 shows the results of the tensile-shear test performed on the FSSW specimen. The HPF steels were hardened using HPF for both non-coated and Al–Si-coated sheets. These specimens were prepared at various dwell times ranging from 3–9 s, while the rotational speed and plunge depth were fixed at 1000 rpm and 1 mm, respectively. For all cases, sound and robust welds were established. The joint strengths of the Al–Si-coated specimens were lower than those of the non-coated specimen, and a higher standard deviation of joint strength was found in the Al–Si-coated specimens. The difference in joint strength can be derived from the difference in fracture mode, which is a result of different hook shapes with respect to presence of coating layer. In the case of the non-coated specimen, the hook was bent and the fracture occurred along the Al matrix, which is much weaker than the HPF steel used (Fig. 12a and c). Fracture occurred across the hook in the case of the Al–Si-coated specimen with a straight hook (Figs. 12b and d).

The Fe–Al–Si IMC layer on steel sheets affected the shape of the hook during the FSSW of Al/steel dissimilar metals, and, consequently, the joint strength of the weldment. The Al–Si coating on the HPF steel surfaces can prevent oxidation and decarburization at the high temperatures required for the HPF process. The Al–Si coating layer changed its composition into an Fe–Al–Si IMC layer due to the diffusion of constituent elements at a temperature higher than the austenitizing temperature of steel, and the thickness of the coating layer increased slightly. Several compositions of Fe–Al–Si IMCs in the coating layer after the HPF process were demonstrated by Fan et al. [32].

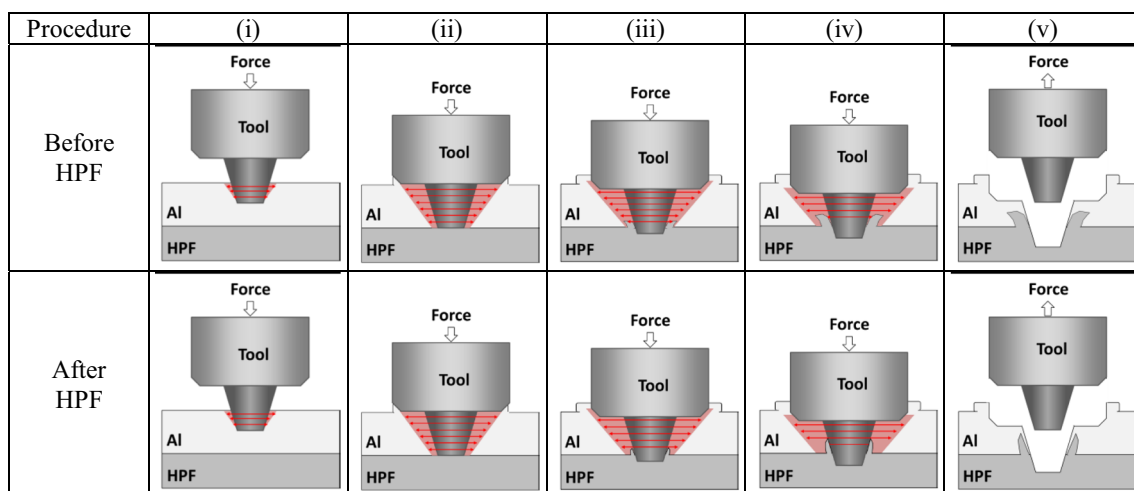| Procedure	(i)	(ii)	(iii)	(iv)	(v)
Before HPF					
After HPF					

Fig. 6 Schematic diagrams of hook generation with the bent or straight upward shape. The red arrows indicate the rotational-tool-induced material flow from the center to away from the tool

Fig. 7 Magnified sectional images of the FSSW specimens. **a** Al/non-coated steel and **b** Al/Al–Si-coated steel (welding conditions: HPF1500 steel after HPF, 1000-rpm rotational speed, 20-mm/min feed rate, 9-s dwell time, and 1-mm plunge depth)
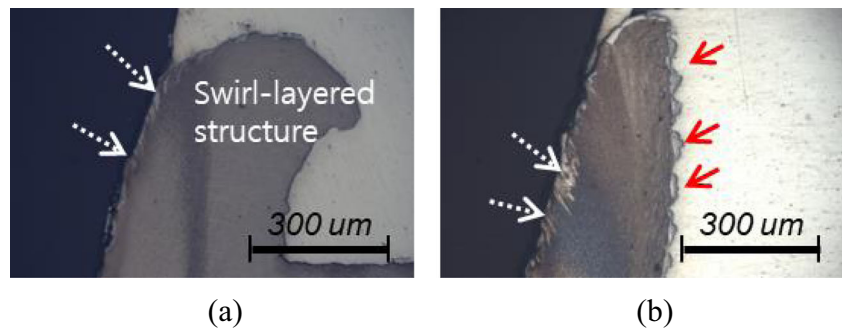
A straight hook shape was observed only when the Fe–Al–Si coating existed on the steel sheet, while bent hooks were found in both non-coated and pure Al–Si-coated specimens. For the pure Al–Si-coated steel sheet, non-HPF specimens were used, and a bent hook was confirmed on the cross-section of the weldment, which coincides with the results of a previous study by da Silva [21]. The formation of Fe–Al–Si coating layer during the HPF process is accompanied by quenching and hardening of the steel sheet. When experiments using different types of steel, such as HPF600 and HPF1500 steel, were compared, it was found that the hook shape was also not affected by the strength of the steel.

The bending of the hook had already occurred when the tool slightly plunged into the lower steel sheet by a small distance (0.3 mm) in the case of specimens without an Fe–Al–Si IMC coating layer (Fig. 5); however, the Fe–Al–Si IMC layer with high hardness interrupted the bending of the hook,

and a straight upward hook was formed for specimens with the Fe–Al–Si coating.

The shape of the Fe–Al–Si coating on the outer surface of the hook was partially serrated (Fig. 7b). The high hardness of the remaining layer of coating caused irregularly high hardness along the hook boundary. This layer had mostly the same composition and thickness as the Fe–Al–Si coating of the unwelded post-HPF specimen. The Fe–Al–Si coating on the inner surface was fully separated from the specimen and scattered within the Al matrix in the SZ. By the diffusion of metals, a newly formed thin Fe–Al IMC layer without Si appeared at the steel hook–Al matrix interface.

In the case of the non-coated specimen, the steel hook can be bent easily because Young's modulus and the yield strength of steel drastically decreased at high temperatures. An Fe–Al IMC layer with high hardness at the interface was observed. However, only a smooth hardness profile could be measured
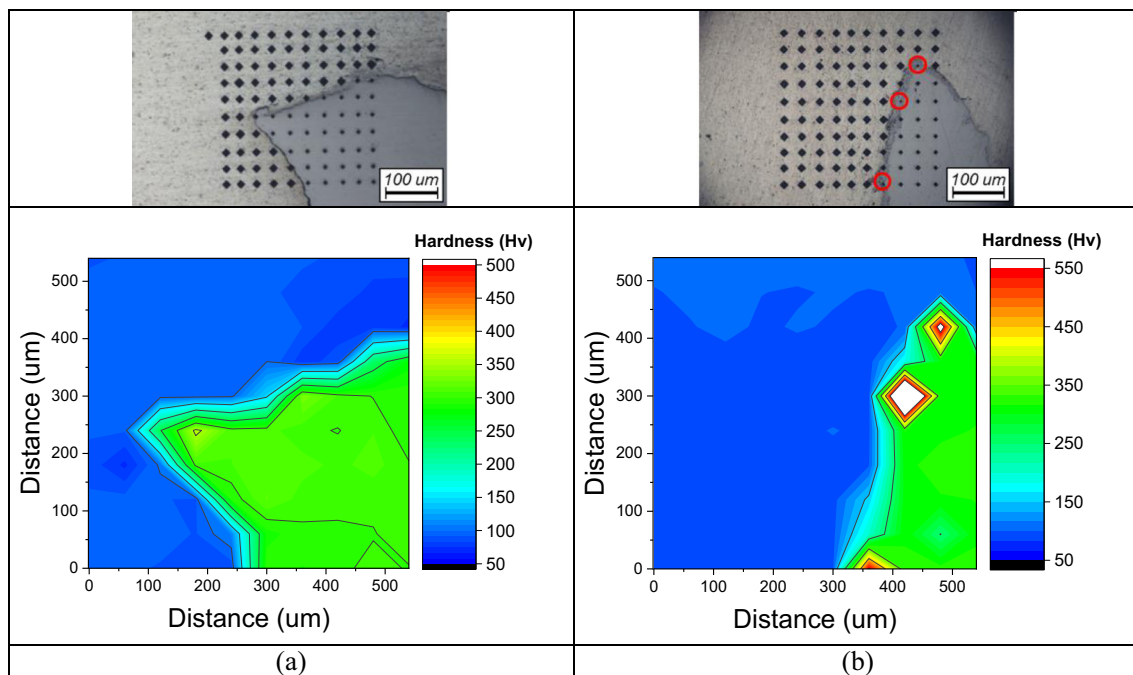

Fig. 8 Hardness maps of the **a** bent hook for non-coated HPF1500 steel and **b** straight hook for Al–Si-coated steel (welding conditions: same as in Fig. 7)

because of the small thickness of the IMC layer (Fig. 8a). In the case of specimens with Al–Si coating, i.e., pre-HPF specimens, the Al–Si layer would easily mix with Al matrix during the FSSW. A 3-μm-thick Fe–Al–Si layer, as shown in Fig. 2c, is decomposed at high temperatures followed by the formation of a new Al–Fe IMC layer that replaces the former Fe–Al–Si coating.

The hook height can influence the fracture mode and joint strength of an Al/steel dissimilar metal joint as shown in a study by Wang et al. [26]. A straight upward hook reduced the joint strength and increased its standard deviation. The fracture location was the root of the hook in straight hook, while for bent hook it was the Al matrix.

During the laser welding of Al–Si-coated HPF steel, the coating layer was diluted into the fusion welds, which degraded the mechanical properties [4, 5, 22]. Similarly, in the FSSW of Al–Si-coated HPF steel, the high-hardness coating layer could modify the steel hook shape and reduce the joint strength. Further studies to optimize the tool shape and process parameters are required to control the hook shape. In addition, a high-hardness tool is necessary to contact and endure the Fe–Al–Si IMC layer.

Fig. 9 Sectional images of the hook formed on the Al–Si-coated HPF1500 steel specimen (**a** macro-section (× 70), **b** macro-section (× 300), and **c**–**h** indicated in (**a**) using a yellow box (welding conditions: same as in Fig. 7)
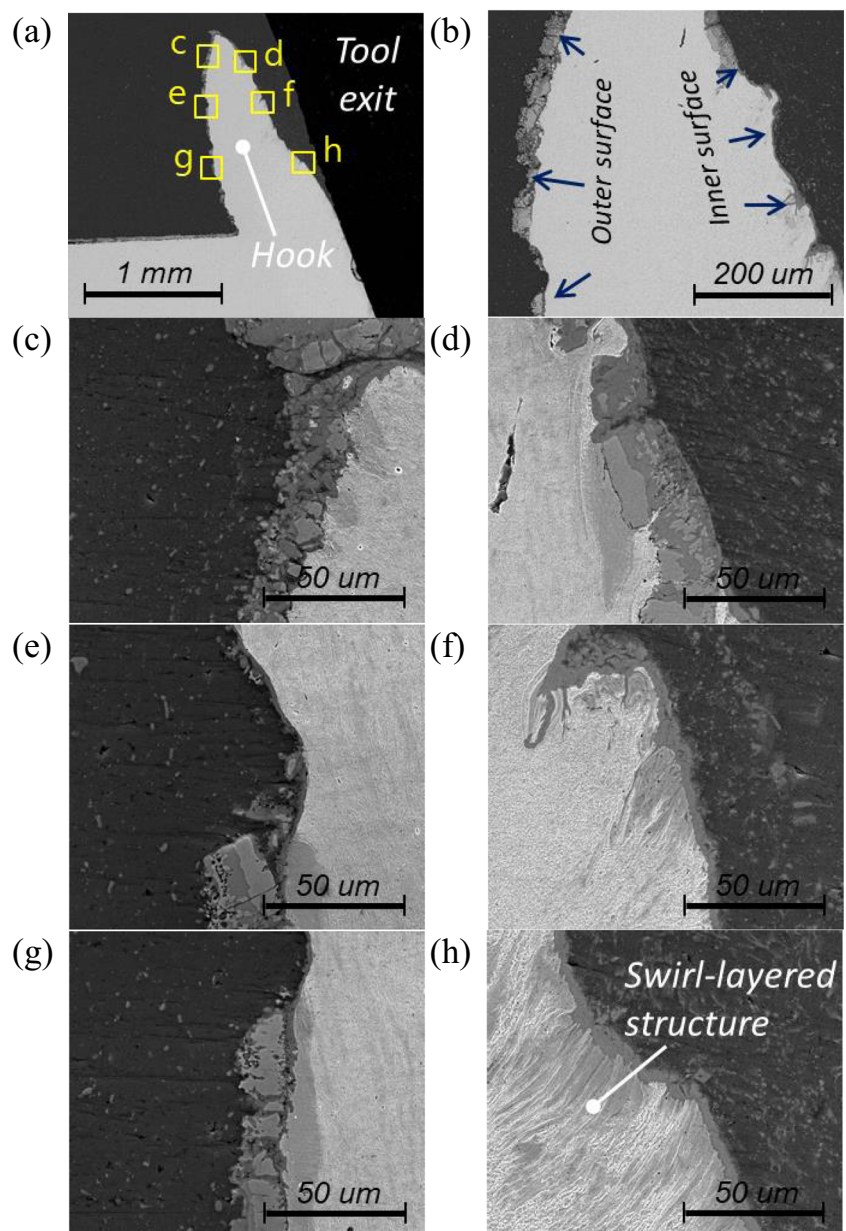
4 Conclusions

In this study, joining of dissimilar material—aluminum alloy and hot-press forming steel—was performed using friction stir spot welding. The effect of Al–Si coating layer on hook formation during the friction stir spot welding was evaluated. HPF steels with and without the Al–Si coating were welded with Al alloy, and the corresponding mechanical and metallurgical properties of the welds were investigated. The following conclusions were derived.

(1) The shape of the hook, which was built-up during the friction stir spot welding, changed with the presence of the Al–Si coating layer and the hot-press forming process. In the case of the pre-HPF specimens, the hook was

bent regardless of the presence of the coating. The straight hook was only formed in the Al–Si-coated specimen after HPF, when the Al–Si coating layer was turned into a brittle Fe–Al–Si IMC layer by the diffusion of metals at high temperature. The hook shape influenced the mechanical properties and fracture mode. It was confirmed that the joint strength of specimens with the straight hook was lower than that of specimens with the bent hook.

(2) The hard Fe–Al–Si IMC layer on the outer surface of the hook was the main cause of the straight hook shape. The HPF process involves heating the metal above the austenite transformation (Ac3) temperature and then quenching it at room temperature. This thermal history transformed the composition of the Al–Si coating layer
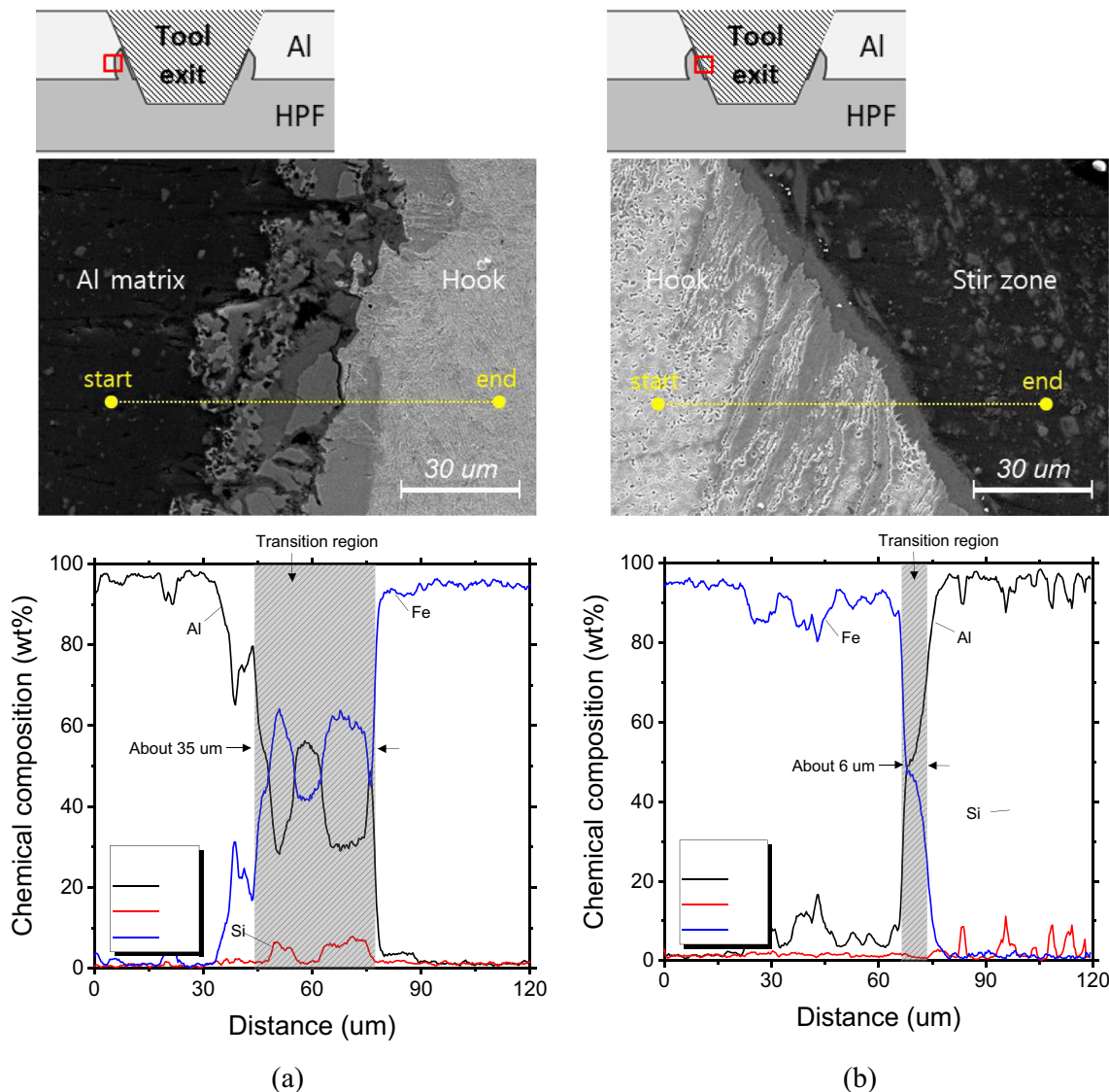

Fig. 10 Measured chemical composition across the **a** outer surface and **b** inner surface of the formed hook (welding conditions: given in Fig. 7)

Fig. 12 Schematic diagram of failure at **a** Al matrix and **b** the hook. Macro-section images of failure specimen at **c** Al matrix and **b** the hook (welding conditions; 1000-rpm rotational speed, 20-mm/min feed rate, 6-s dwell time, and 1-mm plunge depth)
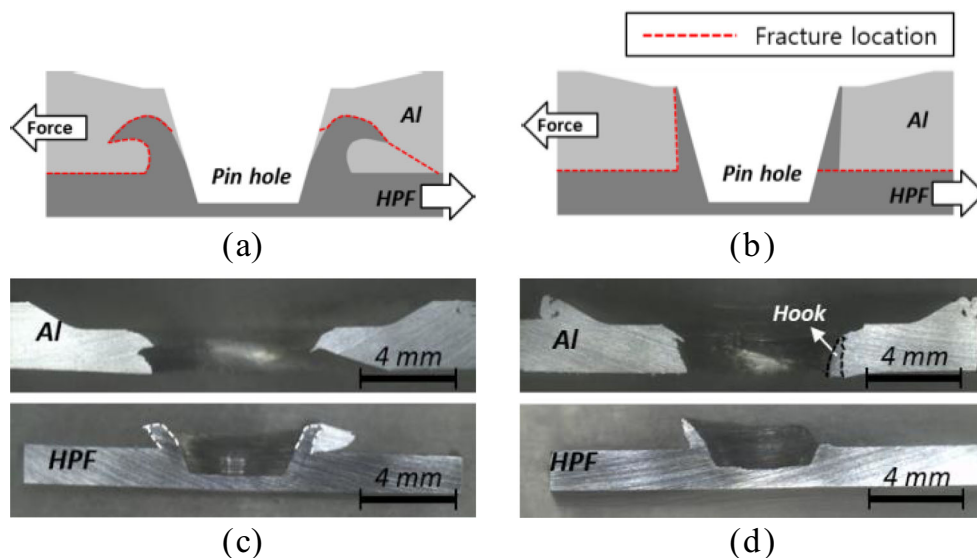
on the HPF steels into Fe–Al–Si, which influenced the hardness profile of the welds and the interface layer distribution, as well as the hook shape. At the inner surface of the hook, between Al and steel, a thin Fe–Al IMC layer was formed, and a swirling Fe–Al layer inside the interface was observed. At the outer surface of the hook, an Fe–Al–Si IMC layer, which has a chemical composition similar to the coating layer prior to the welding, was observed. The hard Fe–Al–Si layer is expected to avert the deformation of the hook during welding. De-coating can improve the joint strength by modifying the hook shape to bent hook.
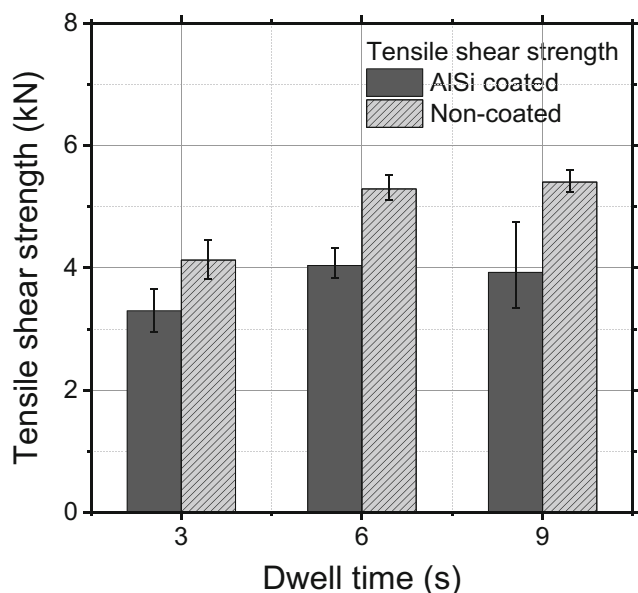

Fig. 11 Measured tensile-shear strengths according to dwell time (welding conditions: 1000-rpm rotational speed, 20-mm/min feed rate, and 1-mm plunge depth)

References

1. Stanford K (2017) Lightweighting boosts vehicle safety. Alum Int Today 30(6):10–12
2. Fan DW, Kim HS, De Cooman BC (2009) A review of the physical metallurgy related to the hot press forming of advanced high strength steel. Steel Res Int 80(3):241–248
3. Karbasian H, Tekkaya AE (2010) A review on hot stamping. J Mater Process Technol 210(15):2103–2118
4. Kim C, Kang M, Park Y (2011) Laser welding of Al-Si coated hot stamping steel. Procedia Eng 10:2226–2231
5. Kim C-H, Choi J-K, Kang M-J, Park Y-D (2010) A study on the CO_2 laser welding characteristics of high strength steel up to 1500 MPa for automotive application. J Achiev Mater Manuf Eng 39(1):79–86
6. Kang M, Kim C (2011) Analysis of laser and resistance spot weldments on press-hardened steel, Mater Sci Forum. Trans Tech Publ 2011(99):202–205
7. Sakayama T, Naito Y, Miyazakki Y, Nose T, Murayma G, Saita K, Oikawa H (2013) Dissimilar metal joining technologies for steel sheet and aluminum alloy sheet in auto body. Nippon Steel Techn Rep 103:91–98
8. Meschut G, Janzen V, Olfermann T (2014) Innovative and highly productive joining technologies for multi-material lightweight car body structures. J Mater Eng Perform 23(5):1515–1523. https://doi.org/10.1007/s11665-014-0962-3
9. Martinsen K, Hu SJ, Carlson BE (2015) Joining of dissimilar materials. CIRP Ann 64(2):679–699. https://doi.org/10.1016/j.cirp.2015.05.006
10. Agudo L, Eyidi D, Schmaranzer CH, Arenholz E, Jank N, Bruckner J, Pyzalla AR (2007) Intermetallic Fe x Al y-phases in a steel/Al-alloy fusion weld. J Mater Sci 42(12):4205–4214
11. He X, Pearson I, Young K (2008) Self-pierce riveting for sheet materials: state of the art. J Mater Process Technol 199(1-3):27–36. https://doi.org/10.1016/j.jmatprotec.2007.10.071
12. Han L, Chrysanthou A (2008) Evaluation of quality and behaviour of self-piercing riveted aluminium to high strength low alloy sheets

with different surface coatings. Mater Des 29(2):458–468. https://doi.org/10.1016/j.matdes.2006.12.020

13. Dilthey U, Stein L (2006) Multimaterial car body design: challenge for welding and joining. Sci Technol Weld Join 11(2):135–142

14. Kimapong K, Watanabe T (2004) Friction stir welding of aluminum alloy to steel. Weld J 83(10):277s–282s

15. Taban E, Gould JE, Lippold JC (2010) Dissimilar friction welding of 6061-T6 aluminum and AISI 1018 steel: properties and microstructural characterization. Mater Des 31(5):2305–2311

16. Kusuda Y (2013) Honda develops robotized FSW technology to weld steel and aluminum and applied it to a mass-production vehicle. Ind Robot Int J 40(3):208–212

17. Mishra RS, Ma Z (2005) Friction stir welding and processing. Mater Sci Eng R Res 50(1-2):1–78

18. Santella M, Hovanski Y, Pan T-Y (2012) Friction stir spot welding (FSSW) of advanced high strength steel (AHSS). SAE Int J Mater Manuf 5(2):382–387

19. Hovanski Y, Santella ML, Grant GJ (2007) Friction stir spot welding of hot-stamped boron steel. Scr Mater 57(9):873–876. https://doi.org/10.1016/j.scriptamat.2007.06.060

20. Hong SH, Sung S-J, Pan J (2015) Failure mode and fatigue behavior of dissimilar friction stir spot welds in lap-shear specimens of transformation-induced plasticity steel and hot-stamped boron steel sheets. J Manuf Sci Eng 137(5):051023

21. da Silva AAM, Aldanondo E, Alvarez P, Arruti E, Echeverría A (2013) Friction stir spot welding of AA 1050 Al alloy and hot stamped boron steel (22MnB5). Sci Technol Weld Join 15(8):682–687. https://doi.org/10.1179/136217110x12785889549462

22. Kang M, Kim C, Lee J (2012) Weld strength of laser-welded hot-press-forming steel. J Laser Appl 24(2):022004

23. Badarinarayan H, Shi Y, Li X, Okamoto K (2009) Effect of tool geometry on hook formation and static strength of friction stir spot welded aluminum 5754-O sheets. Int J Mach Tools Manuf 49(11):814–823. https://doi.org/10.1016/j.ijmachtools.2009.06.001

24. Bozzi S, Helbert-Etter AL, Baudin T, Criqui B, Kerbiguet JG (2010) Intermetallic compounds in Al 6016/IF-steel friction stir spot welds. Mater Sci Eng A 527(16):4505–4509. https://doi.org/10.1016/j.msea.2010.03.097

25. Wang T, Sidhar H, Mishra RS, Hovanski Y, Upadhyay P, Carlson B (2018) Friction stir scribe welding technique for dissimilar joining of aluminium and galvanised steel. Sci Technol Weld Join 23(3):249–255

26. Wang T, Sidhar H, Mishra RS, Hovanski Y, Upadhyay P, Carlson B (2019) Effect of hook characteristics on the fracture behaviour of dissimilar friction stir welded aluminium alloy and mild steel sheets. Sci Technol Weld Join 24(2):178–184. https://doi.org/10.1080/13621718.2018.1503801

27. Xu RZ, Cui SL, Li H, Hou YX, Wei ZC (2019) Improving hook characterization of friction stir lap welded Al alloy joint using a two-section stepped friction pin. Int J Adv Manuf Technol 102(9):3739–3746

28. Derazkola HA, Khodabakhshi F (2019) Intermetallic compounds (IMCs) formation during dissimilar friction-stir welding of AA5005 aluminum alloy to St-52 steel: numerical modeling and experimental study. Int J Adv Manuf Technol 100(9-12):2401–2422

29. Chen YC, Komazaki T, Tsumura T, Nakata K (2008) Role of zinc coat in friction stir lap welding Al and zinc coated steel. Mater Sci Technol 24(1):33–39

30. Ratanathavorn W, Melander A (2017) Influence of zinc on intermetallic compounds formed in friction stir welding of AA5754 aluminium alloy to galvanised ultra-high strength steel. Sci Technol Weld Join 22(8):673–680

31. Santella M, Hovanski Y, Frederick A, Grant G, Dahl M (2010) Friction stir spot welding of DP780 carbon steel. Sci Technol Weld Join 15(4):271–278

32. Fan DW, Kim HS, Oh J-K, Chin K-G, De Cooman B (2010) Coating degradation in hot press forming. ISIJ Int 50(4):561–568

33. Shome M, Tumuluru M (2015) Welding and joining of advanced high strength steels (AHSS), vol 85. Elsevier

34. Yoon J, Kim C, Rhee S (2018) Compensation of vertical position error using a force–deflection model in friction stir spot welding. Metals 8(12):1049

35. Yoon J, Kim C, Rhee S (2019) Performance of plunge depth control methods during friction stir welding. Metals 9(3):283

36. Yang Q, Mironov S, Sato YS, Okamoto K (2010) Material flow during friction stir spot welding. Mater Sci Eng A 527(16):4389–4398. https://doi.org/10.1016/j.msea.2010.03.082

37. Su P, Gerlich A, North T, Bendzsak G (2007) Intermixing in dissimilar friction stir spot welds. Metall Mater Trans A 38(3):584–595

38. Ohishi K, Sakamura M, Ota K, Fujii H (2016) Novel dissimilar spot welding of aluminium alloy and steel sheets by friction stirring. Weld Int 30(2):91–97. https://doi.org/10.1080/09507116.2014.921088